Inorganic Chemistry

Article

pubs.acs.org/IC

New Ternary Germanides $La_4Mg_5Ge_6$ and $La_4Mg_7Ge_6$: Crystal Structure and Chemical Bonding

Pavlo Solokha,[†,*] Serena De Negri,[†] Monika Skrobanska,[†] Adriana Saccone,[†] Volodymyr Pavlyuk,[‡,§] and Davide M. Proserpio[⊥]

[†]Dipartimento di Chimica e Chimica Industriale, Università di Genova, Via Dodecaneso 31, I-16146 Genova, Italy

[‡]Department of Inorganic Chemistry, Ivan Franko National University of Lviv, Kyryla and Mefodiya street 6, 79005 Lviv, Ukraine

[§]Institute of Chemistry and Environment Protection, Jan Dlugosz University, al. Armii Krajowej 13/15, 42200 Czestochowa, Poland

[⊥]Dipartimento di Chimica Strutturale e Stereochimica Inorganica, Università di Milano, Via Venezian 21, 20133 Milano, Italy

Supporting Information

ABSTRACT: The synthesis, structural characterization, and chemical-bonding peculiarities of the two new polar lanthanum−magnesium germanides $La_4Mg_5Ge_6$ and $La_4Mg_7Ge_6$ are reported. The crystal structures of these intermetallics were determined by single-crystal X-ray diffraction analysis. The $La_4Mg_5Ge_6$ phase crystallizes in the orthorhombic $Gd_4Zn_5Ge_6$ structure type [$Cmc2_1$, $oS60$, $Z = 4$, $a = 4.5030(7)$ Å, $b = 20.085(3)$ Å, $c = 16.207(3)$ Å, wR2 = 0.0451, 1470 F^2 values, 93 variables]. The $La_4Mg_7Ge_6$ phase represents a new structure type with a monoclinic unit cell [$C2/m$, $mS34$, $Z = 2$, $a = 16.878(3)$ Å, $b = 4.4702(9)$ Å, $c = 12.660(3)$ Å, $\beta = 122.25(3)°$, wR2 = 0.0375, 1466 F^2 values, 54 variables]. Crystallographic analysis together with linear muffin-tin orbital band structure calculations reveals the presence of strongly bonded 3D polyanionic [Mg−Ge] networks balanced by positively charged La atoms in both stoichiometric compounds. The $La_4Mg_5Ge_6$ compound is related to Zintl phases, showing a prominent density of states pseudogap at the Fermi level. A distinctive feature of the $La_4Mg_5Ge_6$ structure is the presence of Ge−Ge covalent dumbbells; in $La_4Mg_7Ge_6$, the higher Mg content generates a polyanionic network consisting exclusively of Mg−Ge heterocontacts. Nevertheless, the frameworks of the two phases are structurally similar, as is highlighted in this work.

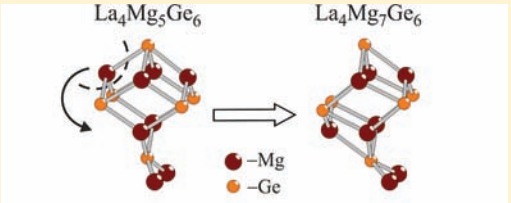

topological relationship for a part of [Mg–Ge] polyanionic frameworks in $La_4Mg_5Ge_6$ and $La_4Mg_7Ge_6$

1. INTRODUCTION

Tetrels are typical elements involved in the formation of binary Zintl phases together with electropositive alkali, alkaline-earth, and rare-earth metals.[1] The Mg_2X (X = Si, Ge, Sn) series is one of the earliest examples of classical Zintl phases, where Mg plays the role of positive counterpart to the isolated, negatively charged X atoms.

A more complex and attractive chemistry is expected to arise from the addition of a third metal competing with Mg as an electropositive component. Nevertheless, this field has not been extensively explored so far. With regard to germanides, a dozen M^{II}−Mg−Ge compounds (M^{II} = divalent metal) were reported,[2] of which the ternary compounds $Sr_{2.2}Mg_{11.8}Ge_7$, $Sr_5Mg_{19}Ge_{12}$, and SrMgGe were ascribed to Zintl phases, highlighting the cation size as an important stabilization factor.[3,4] The RE_2MgGe_2 compounds (RE = rare-earth metal) are almost the only examples of ternary Mg-containing germanides with trivalent metals.[5,6] Crystal structure analysis of these phases and electronic structure calculations performed on Gd_2MgGe_2[6] reveal strong Ge−Ge and Mg−Ge covalent interactions, suggesting that Mg does not act as a positively charged spacer in the structure. In fact, Mg was already reported to take part in the negatively charged network together with the more electronegative element for A−Mg−X ternary polar intermetallics (A = La, K, Ba, Sr; X = Ag, In).[7−10] Here we report the crystal structure and chemical bonding of two novel magnesium germanides, $La_4Mg_5Ge_6$ and $La_4Mg_7Ge_6$, featuring the presence of [Mg−Ge] polyanionic networks.

2. EXPERIMENTAL SECTION

2.1. Synthesis and Scanning Electron Microscopy (SEM)/ Wavelength-Dispersive X-ray Spectroscopy (WDXS) Characterization. Single crystals of $La_4Mg_5Ge_6$ and $La_4Mg_7Ge_6$ were selected from two alloys with nominal compositions $La_{20}Mg_{38}Ge_{42}$ (sample 1) and $La_{16}Mg_{57}Ge_{27}$ (sample 2), respectively. Pure elements were used for the synthesis: 99.9 mass % purity lanthanum and magnesium supplied by NewMet Koch, Waltham Abbey, England, and 99.999 mass % purity germanium supplied by MaTecK GmbH, Jülich, Germany. The weighed constituent metals were enclosed in arc-sealed tantalum crucibles and induction-melted. The melting was performed under a stream of pure argon, and it was repeated several times in order to ensure homogeneity. After melting, the samples were annealed at 500 °C for 25 days and finally quenched.

A JEOL 8200 Super Probe scanning electron microscope equipped with an electron probe microanalysis system based on WDXS was used in order to investigate the microstructure and to perform quantitative analyses.

Received: July 12, 2011
Published: December 7, 2011

dx.doi.org/10.1021/ic2014732 | *Inorg. Chem.* 2012, 51, 207−214

2.2. X-ray Diffraction Measurements and Crystal Structure Determination. Good-quality crystals with metallic luster and size suitable for performing single-crystal measurements were mechanically extracted from the split ingots of samples 1 and 2. Because these alloys are sensitive to air oxidation, they were mounted on glass fibers and then dropped into quick-drying glue. Single-crystal intensity data have been collected by the ω-scan method on a Bruker APEX-II CCD area detector diffractometer (graphite-monochromatized Mo Kα radiation, λ = 0.071073 nm). Empirical absorption corrections (*SADABS*)[11] were applied to all data. Powder X-ray diffraction data were collected by means of a Philips X'Pert MPD diffractometer (Cu Kα radiation; step mode of scanning) in order to ensure the crystal structures of the phases.

Selected crystallographic data and structure refinement parameters for the studied phases are listed in Table 1. The CIF files, containing details of the structure refinement, are available in the Supporting Information. The CIF files have also been deposited with Fachinformationszentrum Karlsruhe, 76344 Eggenstein-Leopoldshafen, Germany: depository numbers CSD-422837 ($La_4Mg_5Ge_6$) and CSD-422838 ($La_4Mg_7Ge_6$). The theoretical powder patterns generated from the single-crystal models correspond well to the observed powder diffraction patterns shown in Figure 1S in the Supporting Information.

Table 1. Crystallographic Data for the $La_4Mg_5Ge_6$ and $La_4Mg_7Ge_6$ Single Crystals and Experimental Details of the Structural Determination

empirical formula	$La_4Mg_5Ge_6$	$La_4Mg_7Ge_6$
WDXS composition	$La_{28.6}Mg_{32.3}Ge_{39.1}$	$La_{24.1}Mg_{42.4}Ge_{33.5}$
structure type	$Gd_4Zn_5Ge_6$	$La_4Mg_7Ge_6$
fw, M_r, g mol^{-1}	1112.73	1161.417
cryst syst	orthorhombic	monoclinic
space group	$Cmc2_1$ (No. 36)	$C2/m$ (No. 12)
Pearson symbol, Z	*o*S60, 4	*m*S34, 2
unit cell dimensions		
a, Å	4.5030(7)	16.878(3)
b, Å	20.085(3)	4.4702(9)
c, Å	16.207(3)	12.660(3)
β, deg		122.25(3)
V, Å^3	1465.8(4)	807.8(3)
calcd density (D_{calc}), g cm^{-3}	5.042	4.874
abs coeff (μ), mm^{-1}	23.661	21.591
total reflns	9328	9817
indep reflns	1470 (R_{int} = 0.0541)	1466 (R_{int} = 0.0274)
reflns with $I > 2\sigma(I)$	1431 (R_{sigma} = 0.0297)	1372 (R_{sigma} = 0.0174)
data/param	1470/93	1466/54
GOF on F^2	1.07	1.13
final R indices [$I > 2\sigma(I)$]	R1 = 0.0192; wR2 = 0.0451	R1 = 0.0186; wR2 = 0.0375
R indices (all data)	R1 = 0.0202; wR2 = 0.0455	R1 = 0.0208; wR2 = 0.0381
$\Delta\rho_{fin}$(max/min), e Å^{-3}	1.73/−0.84	1.17/−1.01

$La_4Mg_5Ge_6$ Compound. Only $h + k = 2n$ reflections were observed in the recorded data set, clearly indicating that this crystal structure possesses a base-centered orthorhombic unit cell. Possible space groups were $Cmc2_1$ (No. 36), *Ama*2 (No. 40), and *Cmcm* (No. 63). The test of the statistical distribution of intensities $|E^2 - 1|$ gives 0.766 with a strong indication of noncentrosymmetrical character. In fact, the adequate structural model was deduced from an automatic interpretation of direct methods with *SHELX-97* package programs[12] in the noncentrosymmetric space group $Cmc2_1$; this model is also associated with the lowest combined figure of merit. Considering the interatomic distances, the located crystallographic positions were assumed to be four La, five Mg, and six Ge sites. The occupancy parameters of all of the crystallographic sites were varied in a separate series of least-squares cycles along with the displacement parameters, but they did not vary more than 3% from full occupation and were assumed to be unity in further cycles.

No higher crystallographic symmetry in the tested model was found by the *ADDSYM* algorithm implemented in *PLATON*.[13] The final structure was then refined with anisotropic displacement parameters.

$La_4Mg_7Ge_6$ Compound. An analysis of the systematic extinctions for the collected data set indicated three possible space groups: *C*2 (No. 5), *Cm* (No. 8), and *C*2/*m* (No. 12). The test of the statistical distribution of intensities $|E^2 - 1|$ (0.955) suggested the centrosymmetric space group *C*2/*m*. The correctness of this space group was confirmed by the lowest combined figure of merit associated with the model obtained with the *SHELX-97* package programs[12] based on

Table 2. Atomic Coordinates and Equivalent Isotropic Displacement Parameters (Å^2) for the $La_4Mg_5Ge_6$ Single Crystal

atom	Wyckoff site	site	x/a	y/b	z/c	U_{eq}[25]
La1	4a	*m*..	0	0.0141(1)	0.2639(1)	0.0103(2)
La2	4a	*m*..	0	0.0317(1)	0.0012(1)	0.0094(2)
La3	4a	*m*..	0	0.1662(1)	0.4613(1)	0.0094(2)
La4	4a	*m*..	0	0.1753(1)	0.8211(1)	0.0097(2)
Ge1	4a	*m*..	0	0.1132(1)	0.6439(1)	0.0103(2)
Ge2	4a	*m*..	0	0.2244(1)	0.2837(1)	0.0097(3)
Ge3	4a	*m*..	0	0.2300(1)	0.0000(1)	0.0095(3)
Ge4	4a	*m*..	0	0.4340(1)	0.3654(1)	0.0097(3)
Ge5	4a	*m*..	0	0.5556(1)	0.4127(1)	0.0102(3)
Ge6	4a	*m*..	0	0.5718(1)	0.1377(1)	0.0091(2)
Mg1	4a	*m*..	0	0.1552(2)	0.1405(3)	0.0126(7)
Mg2	4a	*m*..	0	0.3013(2)	0.1438(3)	0.0144(8)
Mg3	4a	*m*..	0	0.3407(2)	0.4987(3)	0.0103(9)
Mg4	4a	*m*..	0	0.4414(2)	0.0970(3)	0.0173(9)
Mg5	4a	*m*..	0	0.6499(2)	0.2834(3)	0.0133(10)

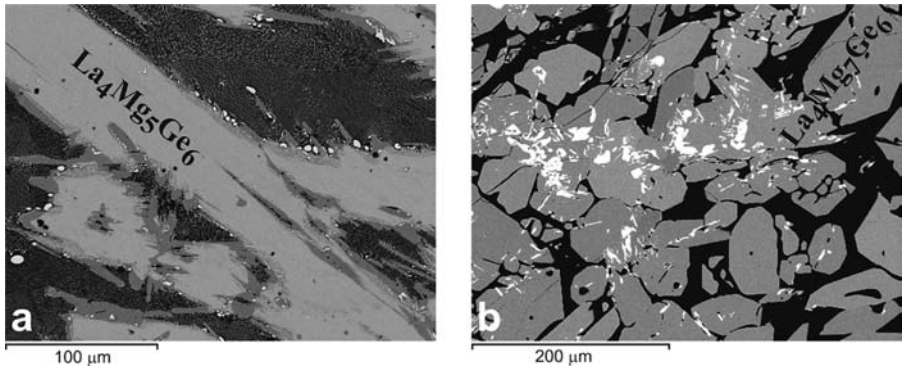

Figure 1. SEM images (BSE mode) of the alloys, from which the $La_4Mg_5Ge_6$ (sample 1, a) and $La_4Mg_7Ge_6$ (sample 2, b) single crystals were taken for X-ray diffraction analysis.

dx.doi.org/10.1021/ic2014732 | *Inorg. Chem.* 2012, 51, 207−214

Table 3. −iCOHPs (eV per Bond per Cell) at E_F for the Strongest Contacts within the First Coordination Spheres in $La_4Mg_5Ge_6$

central atom	adjacent atoms	d (Å)	−iCOHP	central atom	adjacent atoms	d (Å)	−iCOHP	central atom	adjacent atoms	d (Å)	−iCOHP
La1−	1Ge1	3.212(2)	1.31	Mg1−	1Ge2	2.706(5)	1.36	Ge1−	2Mg4	2.617(2)	1.83
	2Ge4	3.219(1)	1.18		1Ge3	2.728(5)	1.38		2Mg2	2.832(2)	1.41
	2Ge6	3.255(1)	1.03		2Ge6	2.807(2)	1.24		1La4	3.131(2)	1.33
	2Ge5	3.404(1)	0.83		1Mg2	2.934(5)	0.40		1La3	3.145(2)	1.39
	1Mg1	3.468(4)	0.37		2Mg3	3.218(5)	0.26		1La1	3.212(2)	1.31
	2Mg5	3.551(3)	0.38		2Mg5	3.232(5)	0.24		1La2	3.718(2)	0.61
	2Mg4	3.810(4)	0.24		1La2	3.353(4)	0.40				
	1La4	3.915(1)	0.38		1La1	3.468(4)	0.37	Ge2−	2Mg5	2.704(2)	1.74
	1La2	3.955(1)	0.34						1Mg1	2.706(5)	1.36
				Mg2−	1Ge3	2.735(5)	1.63		1Mg2	2.743(5)	1.56
La2−	2Ge5	3.193(1)	1.13		1Ge2	2.743(5)	1.56		2La4	3.081(1)	1.37
	2Ge4	3.223(1)	1.08		2Ge1	2.832(2)	1.41		1La3	3.107(2)	1.40
	2Ge6	3.257(1)	0.97		1Mg4	2.915(6)	0.60				
	2Mg4	3.282(3)	0.42		1Mg1	2.934(5)	0.40	Ge3−	2Mg3	2.662(2)	1.82
	1Mg1	3.353(4)	0.40		2La4	3.681(4)	0.29		1Mg1	2.728(5)	1.38
	2Mg3	3.412(3)	0.43		2La3	3.774(4)	0.28		1Mg2	2.735(5)	1.63
	1Ge1	3.718(2)	0.61						1La4	3.101(2)	1.34
	1La1	3.955(1)	0.34	Mg3−	2Ge3	2.662(2)	1.82		2La3	3.132(1)	1.39
	1Ge3	3.982(1)	0.33		1Ge6	2.858(5)	1.19		1La2	3.982(1)	0.33
	1La3	4.028(1)	0.34		1Ge4	2.861(5)	1.30				
					2Mg1	3.218(5)	0.26	Ge4−	1Ge5	2.558(2)	2.36
La3−	1Ge2	3.107(2)	1.40		2La2	3.412(3)	0.43		1Mg3	2.861(5)	1.30
	2Ge3	3.132(1)	1.39		1La3	3.555(4)	0.38		2La1	3.219(1)	1.18
	1Ge1	3.145(2)	1.39		2La4	3.669(4)	0.32		2La2	3.223(1)	1.08
	2Ge5	3.261(1)	1.18						2La4	3.227(1)	1.18
	1Mg3	3.555(4)	0.38	Mg4−	2Ge1	2.617(2)	1.83				
	2Mg5	3.673(4)	0.35		1Ge6	2.700(4)	1.53	Ge5−	1Ge4	2.558(2)	2.36
	2Mg2	3.774(4)	0.28		1Mg2	2.915(6)	0.60		1Mg5	2.826(5)	1.45
	2Mg4	3.818(4)	0.25		1Ge5	2.987(5)	1.00		1Mg4	2.987(5)	1.00
	1La2	4.028(1)	0.34		2La2	3.282(3)	0.42		2La2	3.193(1)	1.13
					2La1	3.810(4)	0.24		2La3	3.261(1)	1.18
La4	2Ge2	3.081(1)	1.37		2La3	3.818(4)	0.25		2La1	3.404(1)	0.83
	1Ge3	3.101(2)	1.34								
	1Ge1	3.131(2)	1.33	Mg5−	2Ge2	2.704(2)	1.74	Ge6−	1Mg4	2.700(4)	1.53
	2Ge4	3.227(1)	1.18		1Ge5	2.826(5)	1.45		2Mg1	2.807(2)	1.24
	1Mg5	3.563(4)	0.34		1Ge6	2.835(5)	1.29		1Mg5	2.835(5)	1.29
	2Mg3	3.669(4)	0.32		2Mg1	3.232(5)	0.24		1Mg3	2.858(5)	1.19
	2Mg2	3.681(4)	0.29		2La1	3.551(3)	0.38		2La1	3.255(1)	1.03
	1La1	3.915(1)	0.38		1La4	3.563(4)	0.34		2La2	3.257(1)	0.97
	1La2	4.103(1)	0.31		2La3	3.673(4)	0.35				

direct methods. The accepted structural model matches well with the composition expected from SEM/WDXS and contains two La, four Mg, and three Ge sites. Any statistical mixture was revealed in these sites, and the distribution of isotropic thermal parameters was flat. In the final cycles, the anisotropic displacement parameters were refined for all atoms.

2.3. Electronic Structure Calculations. Electronic band structures of the two phases were calculated by the tight-binding, linear muffin-tin orbital (TB-LMTO) method with the atomic spheres approximation (ASA)[14−16] using the *TB-LMTO-ASA 4.7* program.[17] Electronic energies were calculated via density functional theory based on the local density approximation for the exchange-correlation functional, as parametrized by von Barth and Hedin.[18] In the ASA method, space is filled with overlapping Wigner−Seitz spheres; to achieve space filling with orbital overlapping values smaller than 10%, one empty sphere was included for both models, whose position was deduced automatically by an implemented algorithm. The electronic structure calculations were carried out using the non-spin-polarized approach, with enough dense k-point mesh in the irreducible Brillouin zones of the crystallographic unit cell. Self-consistency was achieved when the total energy change was smaller than 1×10^{-5} Ry. Chemical-bonding analyses were based on the density of states (DOS), the crystal orbital Hamilton population (COHP) curves,[19] and the integrated COHP (iCOHP) values. The chemical bonding was analyzed in direct space using the electron-localization function (ELF).[20] Graphics concerning electronic structure calculations were generated by *wxDragon*.[21]

3. RESULTS AND DISCUSSION

3.1. Sample Characterization by SEM/WDXS Analysis. Samples 1 and 2 were originally prepared and characterized with the aim of studying phase relationships of the La−Mg−Ge system at 500 °C. Despite the nominal compositions of both alloys being rather different from the correct stoichiometries of the title germanides, the final yields of the new compounds and the dimensions of their grains allowed subsequent structural analysis.

On the basis of SEM/WDXS analyses, sample 1 contains large crystals of $La_4Mg_5Ge_6$ (>200 μm) surrounded by the $La_4Mg_7Ge_6$ phase (Figure 1a). Two more phases have been detected in this sample, namely, $LaGe_{2-x}$ (white) and Mg_2Ge

dx.doi.org/10.1021/ic2014732 | Inorg. Chem. 2012, 51, 207−214

(black). Sample 2 shows large gray crystals of $La_4Mg_7Ge_6$ (>100 μm), in some of which white residuals of La_2MgGe_2 are detectable (Figure 1b); in the black matrix, Mg and Mg_2Ge were detected.

3.2. Crystal Structure and Chemical-Bonding Analysis. *$La_4Mg_5Ge_6$ Compound.* The refined positional parameters of $La_4Mg_5Ge_6$ standardized by the *STRUCTURE TIDY* program[22] are listed in Table 2. The unit cell consists of 60 atoms occupying 15 Wyckoff sites all of *m..* symmetry. The base-centered structure of this compound is built up of two identical alternating atomic layers shifted at ($^1/_2$, $^1/_2$, 0) with respect to each other. More structural details are presented in the next paragraph. According to Pearson's crystal data compilation,[2] $La_4Mg_5Ge_6$ crystallizes in the $Gd_4Zn_5Ge_6$ structure type, which was solved and described by Kranenberg et al.[23] An interesting feature of these structures is the presence of Ge−Ge dumbbells with distances of 2.56 Å for $La_4Mg_5Ge_6$ (see Table 3) and 2.51 Å for $Gd_4Zn_5Ge_6$.[23] Structural Ge_2 motifs were also shown in the RE_2MgGe_2 series (RE = rare-earth metal), characterized by similar distances (2.54 Å for RE = La).[5] Each Mg atom in the $La_4Mg_5Ge_6$ structure is surrounded by four Ge atoms, forming a slightly distorted tetrahedron; most of the Ge−Mg distances range from 2.62 to 2.99 Å (Table 3), suggesting a strong bonding interaction between these two constituents. The La−Mg and La−Ge distances are spread over a wide range (from 3.02 to 3.77 Å).

In order to deeply investigate the chemical bonding within this germanide, the electronic structure of $La_4Mg_5Ge_6$ was computed using the experimental data listed in Table 2. The total and projected DOSs of $La_4Mg_5Ge_6$ calculated by the TB-LMTO-ASA method are shown in Figure 2 with the Fermi level set as a reference point at 0 eV. The DOS curve is characterized by a pseudogap at the Fermi level, which is a strong indication of the presence of covalent bonds. In the valence band, a clear separation is observed between the s and p orbitals of Ge: the former almost exclusively contribute to the low-energy DOS peaks in the −10 to −7 eV range, and the latter are mixed with La and Mg orbitals in the region from −6 eV to the Fermi level. It has to be noted that both s and p orbitals of Mg contribute to the bonding; instead, La behaves as a typical electropositive element participating with its s and d orbitals. The empty La f states give a wide prominent peak in the conduction band from 2.5 to 3.5 eV, corresponding to the 4f resonance in La.[24]

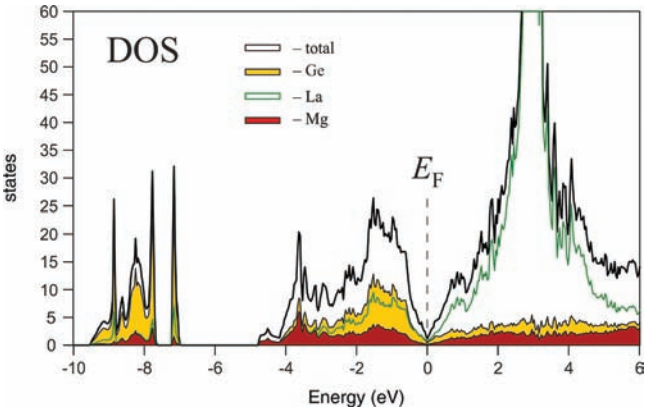

Figure 2. Total and projected DOSs for $La_4Mg_5Ge_6$ (E_F is set at 0 eV).

The localization of electrons can be conveniently visualized by means of ELF plots (Figure 3a,b). The higher electron concentrations (red regions) within the crystal space are observed around Ge atoms, which represent the most electronegative component. Moreover, a significant electron density is localized between Ge4 and Ge5 (ELF ≈ 0.75), supporting the existence of the covalent homonuclear bond, which can also be deduced from the short interatomic distance between them.

As expected from DOS analysis, La and Mg play somewhat different roles in the compound. An extended isotropic area of zero electron localization is observed (blue regions) around La atoms; however, Mg atoms are surrounded by higher electron density zones especially toward Ge atoms. On the basis of these results, it is reasonable to outline in this compound a polyanionic $_\infty[Mg_5Ge_6]^{\delta-}$ framework balanced by La ions (see Figure 3). To quantitatively evaluate the bond strength between the different types of atoms in $La_4Mg_5Ge_6$, COHP and iCOHP were calculated (Figure 4 and Table 3). In the −COHP curves, positive values correspond to bonding interactions, whereas negative values indicate antibonding ones.

The Ge−Ge COHP diagram shows a sharp antibonding peak at low energies, which can be related to the repulsive forces between the closely located Ge4−Ge5 species. This antibonding character is compensated for by La−Ge and Mg−Ge interactions, which constitute a positive counterpart of the antibonding Ge−Ge peak and stabilize Ge_2 dumbbells within the crystal space. However, this covalent bond is associated with the highest iCOHP value in the structure (2.36 eV per bond per cell). A similar behavior was highlighted for $Gd_4Zn_5Ge_6$[23] and Gd_2MgGe_2,[6] where

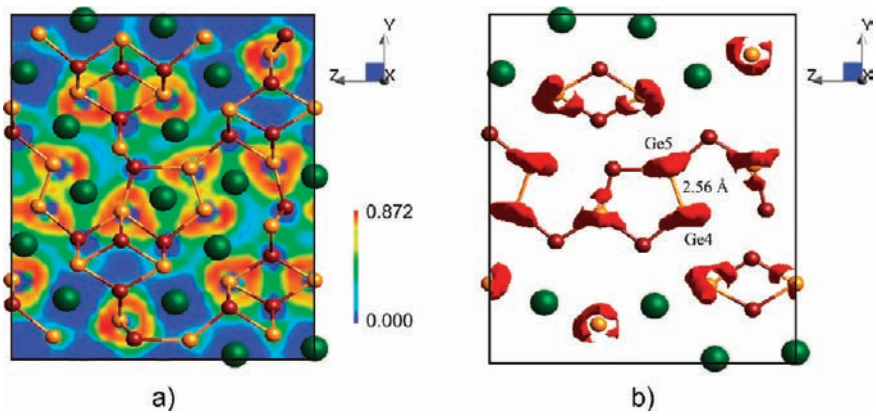

Figure 3. Polyanionic [Mg−Ge] network in $La_4Mg_5Ge_6$ together with (a) the ELF contour plot mapped on the (0, 0, 0) basal plane and (b) 3D isosurfaces of the ELF (η = 0.90) around atoms in the same plane.

dx.doi.org/10.1021/ic2014732 | *Inorg. Chem.* 2012, 51, 207−214

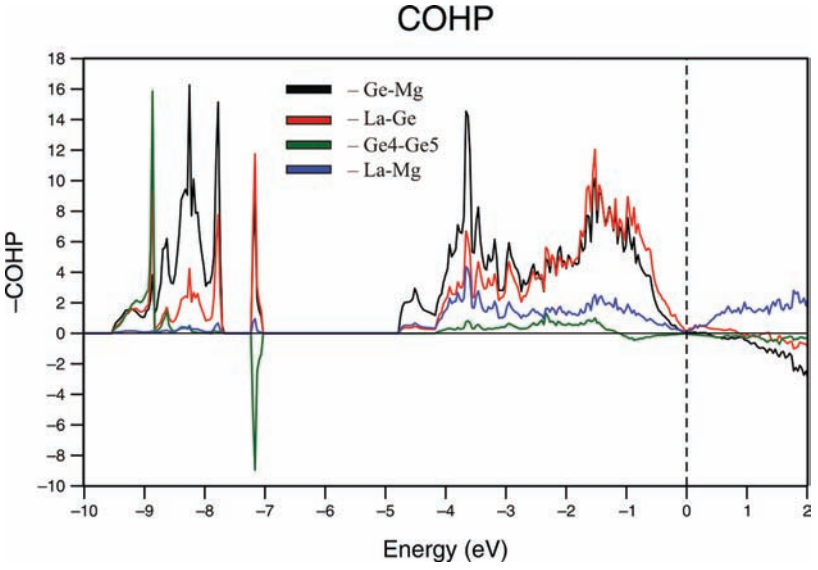

Figure 4. COHPs per bond for $La_4Mg_5Ge_6$ from LMTO calculations.

Table 4. Atomic Coordinates and Equivalent Isotropic Displacement Parameters (Å^2) for the $La_4Mg_7Ge_6$ Single Crystal

atom	Wyckoff site	site	*x*/*a*	*y*/*b*	*z*/*c*	U_{eq}[26]
La1	4i	*m*	0.37003(2)	0	0.15966(2)	0.0094(1)
La2	4i	*m*	0.26627(2)	0	0.38746(2)	0.0094(1)
Ge1	4i	*m*	0.14871(3)	0	0.02819(4)	0.0098(1)
Ge2	4i	*m*	0.11938(3)	0	0.64961(4)	0.0096(1)
Ge3	4i	*m*	0.60600(3)	0	0.30955(4)	0.0106(1)
Mg1	4i	*m*	0.0603(1)	0	0.39472(14)	0.0116(3)
Mg2	4i	*m*	0.68866(11)	0	0.15461(14)	0.0142(3)
Mg3	4i	*m*	0.03826(11)	0	0.13742(14)	0.0151(3)
Mg4	2d	2/*m*	0	$^1/_2$	$^1/_2$	0.0134(4)

Table 5. −iCOHPs (eV per Bond per Cell) at E_F for the Strongest Contacts within the First Coordination Spheres in $La_4Mg_7Ge_6$

central atom	adjacent atoms	*d* (Å)	−iCOHP	central atom	adjacent atoms	*d* (Å)	−iCOHP	central atom	adjacent atoms	*d* (Å)	−iCOHP
La1−	2Ge1	3.154(1)	1.25	Ge2−	1Mg1	2.774(2)	1.36	Mg2−	2Ge1	2.619(1)	1.96
	1Ge1	3.176(1)	1.24		1Mg1	2.824(2)	1.24		1Ge2	2.841(2)	1.28
	2Ge2	3.225(1)	1.05		1Mg2	2.841(2)	1.28		1Ge3	2.952(2)	1.02
	1Ge3	3.376(1)	0.91		2Mg4	2.927(1)	1.08		2Mg3	3.301(2)	0.24
	1Mg2	3.550(2)	0.37		2La2	3.148(1)	1.19		2La2	3.359(1)	0.45
	1Mg4	3.646(2)	0.32		2La1	3.225(1)	1.05		1La1	3.550(2)	0.37
	2Mg1	3.737(1)	0.28						2La1	3.763(2)	0.28
	2Mg3	3.740(1)	0.29	Ge3−	2Mg1	2.764(1)	1.44				
	2Mg2	3.763(2)	0.28		2Mg3	2.897(1)	1.23	Mg3−	1Ge1	2.701(2)	1.77
					1Mg2	2.952(2)	1.02		1Ge1	2.853(2)	1.27
La2−	2Ge2	3.148(1)	1.19		2La2	3.231(1)	1.07		2Ge3	2.897(1)	1.23
	2Ge3	3.231(1)	1.07		1La2	3.246(1)	1.08		1Mg3	2.997(3)	0.40
	1Ge3	3.246(1)	1.08		1La1	3.376(1)	0.91		1Mg1	3.075(3)	0.46
	2Mg2	3.359(1)	0.45		1Mg4	3.690(1)	0.22		2Mg2	3.301(2)	0.24
	1Mg4	3.405(1)	0.42						1La2	3.439(2)	0.42
	1Mg3	3.439(2)	0.42	Mg1−	2Ge3	2.764(1)	1.44		2La1	3.740(2)	0.29
	1Mg1	3.526(2)	0.40		1Ge2	2.774(2)	1.36				
	2Mg1	3.543(1)	0.40		1Ge2	2.824(2)	1.24	Mg4−	4Ge2	2.928(1)	1.08
					2Mg4	3.042(1)	0.46		4Mg1	3.042(2)	0.46
Ge1−	2Mg2	2.619(1)	1.96		1Mg3	3.075(3)	0.46		2La2	3.405(1)	0.42
	1Mg3	2.701(2)	1.77		1La2	3.526(2)	0.40		2La1	3.646(1)	0.32
	1Mg3	2.853(2)	1.27		2La2	3.543(1)	0.40		2Ge3	3.690(1)	0.22
	2La1	3.154(1)	1.25		2La1	3.737(2)	0.28				
	1La1	3.176(1)	1.24								

dx.doi.org/10.1021/ic2014732 | *Inorg. Chem.* 2012, 51, 207−214

identical Ge_2 dimers exist. Strong Mg−Ge interactions are also highlighted both by the corresponding COHP curve, showing only bonding character under E_F, and by the integrated COHP values (Table 3). A noticeable contribution to the total bonding is given by La−Ge contacts, which indeed are generally slightly weaker than the Mg−Ge contacts (Table 3). The homo- and heteroatomic contacts between the electropositive constituents (La and Mg) are the weakest; as an example, the La−Mg COHP curve is shown in Figure 4.

For the $Gd_4Zn_5Ge_6$ structural prototype, the ionic formula splitting $(Gd^{3+})_4(Zn^{2+})_5(Ge^{3-})_2(Ge^{4-})_4$ was proposed in the literature,[23] ascribing this compound to Zintl phases. However, this formula does not take into account Ge atoms forming five Ge−Mg contacts or the different number of heterocontacts of the Ge atoms in the dumbbell. The inadequacy of the Zintl formalism to account for the electronic requirement of the polyanionic networks was discussed for different systems.[26,27] On the other hand, the pseudogap occurring at the Fermi energy in the DOS curves indicates an ideal number of valence electrons for both $Gd_4Zn_5Ge_6$ and $La_4Mg_5Ge_6$, so that they can be considered as related to Zintl phases.

$La_4Mg_7Ge_6$ Compound. The refined positional parameters of $La_4Mg_7Ge_6$ standardized by the *STRUCTURE TIDY* program[22] are listed in Table 4. This compound crystallizes with the monoclinic space group $C2/m$, adopting a new structure type. In the unit cell, 34 atoms are distributed among 9 Wyckoff sites, with all of the m symmetry except for the 2d site ($2/m$ symmetry) occupied by a Mg atom. Similar to the previous compound, also the two-layer structure of $La_4Mg_7Ge_6$ is formed by alternating identical atomic layers shifted at ($^1/_2$, $^1/_2$, 0) with respect to each other. Ge−Ge dumbbells or other direct Ge−Ge contacts do not occur in the $La_4Mg_7Ge_6$ crystal structure. The shortest distances are associated with Ge−Mg contacts, ranging from 2.62 to 2.95 Å (Table 5).

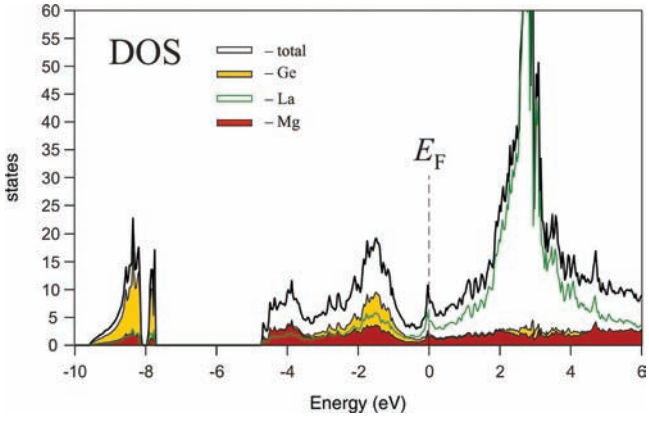

Figure 5. Total and projected DOSs for $La_4Mg_7Ge_6$ (E_F is set at 0 eV).

Each Mg atom in this structure is surrounded by four Ge atoms, forming a slightly distorted tetrahedron (around Mg atoms in the 4i sites) or a rectangle with distances of 2.93 Å (around Mg atoms in the 2d site). The La−Mg and La−Ge distances are distributed between 3.15 and 3.76 Å. The distance distribution of each contact type is comparable to that in $La_4Mg_5Ge_6$, suggesting a similar chemical-bonding picture.

The projected DOS curves of the two compounds (Figures 3 and 5) have the same character, indicating a similar contribution of the constituents to chemical bonding. Nevertheless, fundamental differences in the total DOS curve of $La_4Mg_7Ge_6$, with respect to that of $La_4Mg_5Ge_6$, lie in the absence of a pronounced pseudogap at the Fermi level and the vanishing of the two sharp peaks at about −9 and −7 eV, originating in the latter covalently bonded Ge atoms. These features confirm that no covalent Ge−Ge bonds occur in the structure, as was already deduced from the interatomic distance analysis. Nevertheless, the existence of a $_\infty[Mg_7Ge_6]^{\delta-}$ polyanionic network related to $_\infty[Mg_5Ge_6]^{\delta-}$ (see the next paragraph) is demonstrated by the ELF plots (Figure 6a,b), showing higher electron localization between Ge and Mg, more so on the former naturally, and a wide area of zero electron density around La atoms.

The presence of strong Mg−Ge and La−Ge bonds in $La_4Mg_7Ge_6$ is indicated by both COHP curves (Figure 7) and iCOHP values (Table 5). The COHP curves of these contacts are optimized at the Fermi level, where they change their character from bonding to antibonding type. All of the other contacts are weak in this compound; as an example, the La−Mg COHP curve is shown in Figure 7.

Considering its structural and bonding features, the $La_4Mg_7Ge_6$ can be defined as a polar intermetallic compound.

3.3. Structural Similarities of [M−Ge] (M = Mg, Zn, In) Polyanionic Networks in Germanides. Both germanides studied in this work are characterized by a RE/Ge ratio equal to 2:3; their compositions (and corresponding crystal structures) have been schematically located along the concentration line, which links the hypotetic RE_2Ge_3 compound to pure Mg (Figure 8). The outlined polyanionic frameworks feature two topologically similar structural blocks indicated as **I** and **II**; a slight displacement of a Mg atom is sufficient to transform block **I** into block **II** as shown in the right part of Figure 8. These structural motifs are spaced out by Ge−Ge dumbbells linking three blocks **I** in $La_4Mg_5Ge_6$ and by Mg-centered $MgGe_4$ planar fragments joining four blocks **II** in $La_4Mg_7Ge_6$.

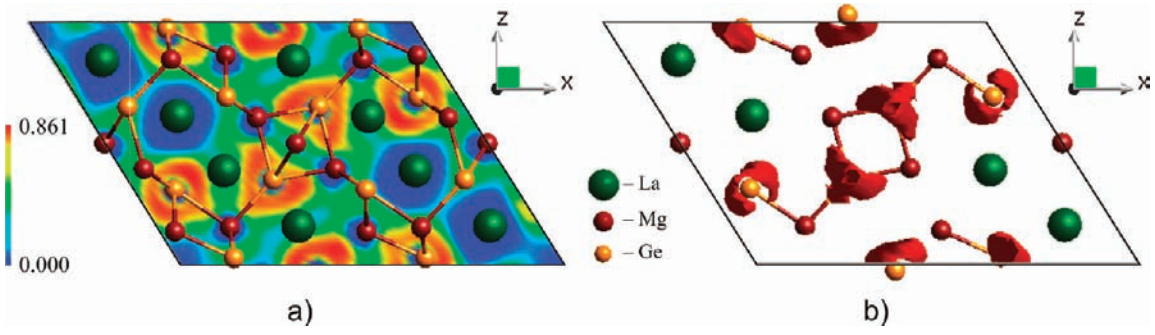

Figure 6. Polyanionic [Mg−Ge] network in $La_4Mg_7Ge_6$ together with (a) the ELF contour plot mapped on the (0, $^1/_2$, 0) plane and (b) 3D isosurfaces of the ELF (η = 0.90) around atoms in the same plane.

dx.doi.org/10.1021/ic2014732 | *Inorg. Chem.* 2012, 51, 207−214

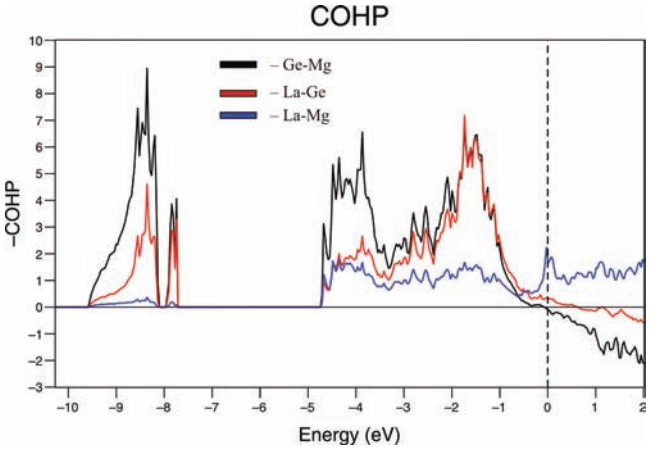

Figure 7. COHPs per bond for $La_4Mg_7Ge_6$ from LMTO calculations.

Because Zn and Mg play similar roles in the isostructural $La_4(Mg\ or\ Zn)_5Ge_6$ phases, the RE–Zn–germanides were also considered to highlight crystal structure similarities. Among several such compounds found in Pearson's database,[2] the $Yb_2Zn_3Ge_3$ phase shows the same RE/Ge ratio and an intermediate content of the third element with respect to the two La–Mg–germanides (Figure 8). In the outlined [Zn–Ge] framework, structural block **II**, topologically identical with that found in $La_4Mg_7Ge_6$, is evident. However, in the $Yb_2Zn_3Ge_3$ crystal structure, four blocks **II** are interconnected by Ge–Ge dumbbells, similarly to $La_4Mg_5Ge_6$. For these reasons, this Yb–Zn–germanide could be viewed as a bridge between the two structures studied in this work.

These structures show similarities to the numerous family of ternary and quaternary In-containing germanides.[28−30] For all of these compounds, the M element (M = Mg, Zn, In) is surrounded by the four closest Ge neighbors in the form of either tetrahedra or rectangles. Only one of these units is observed in some structures (e.g., $RE_4(Mg/Zn)_5Ge_6$, RE_2MgGe_2), whereas both units coexist in others [e.g., $La_4Mg_7Ge_6$, $(Sr,Ca)_5In_3Ge_6$]. The M–Ge heterocontacts in tetrahedra are generally associated with stronger bonds than those in planar fragments, which also agrees with the respective distance contractions.

4. CONCLUSIONS

On the basis of crystallographic analysis and LMTO electronic structure calculations, the $La_4Mg_5Ge_6$ and $La_4Mg_7Ge_6$ novel phases have been interpreted as $_\infty[Mg–Ge]^{\delta-}$ polyanionic frameworks balanced by La cations. The La atoms do not simply act as electron donors but are strongly involved in the overall bonding by polar La–Ge interactions. The negatively charged networks of the two compounds consist of topologically similar structural blocks made up of Mg–Ge contacts but joined in different ways; in $La_4Mg_5Ge_6$, the connection is provided by strongly bonded Ge–Ge dumbbells; however, in $La_4Mg_7Ge_6$, no homonuclear bonds exist and the building blocks are linked by $MgGe_4$ planar units.

The $La_4Mg_5Ge_6$ compound can be associated with Zintl phases, as shown by the DOS pseudogap at the Fermi level and the existence of covalent Ge_2 dumbbells. The increase in the content of reducing agent Mg by two atoms per formula unit in $La_4Mg_7Ge_6$ breaks up the condensed Ge–Ge and changes the bonding character. This is reflected in a less pronounced DOS pseudogap below the Fermi level and leads to the definition of this compound as "polar intermetallic" rather than a Zintl phase.

The structural and bonding characteristics of the studied compounds make them very similar to several already known ternary and quaternary germanides containing Zn or In, confirming a similar role of Mg in stabilizing the polyanionic network together with the more electronegative Ge atoms. Therefore, it could be expected that a wide, mostly unexplored family of Mg-containing germanides exists, whose members can be obtained, for example, by changing the composition and/or the nature of the most electropositive metals. Such exploration will be a goal of our future work.

■ ASSOCIATED CONTENT

Supporting Information

X-ray crystallographic files in CIF format and powder X-ray diffraction patterns. This material is available free of charge via the Internet at http://pubs.acs.org.

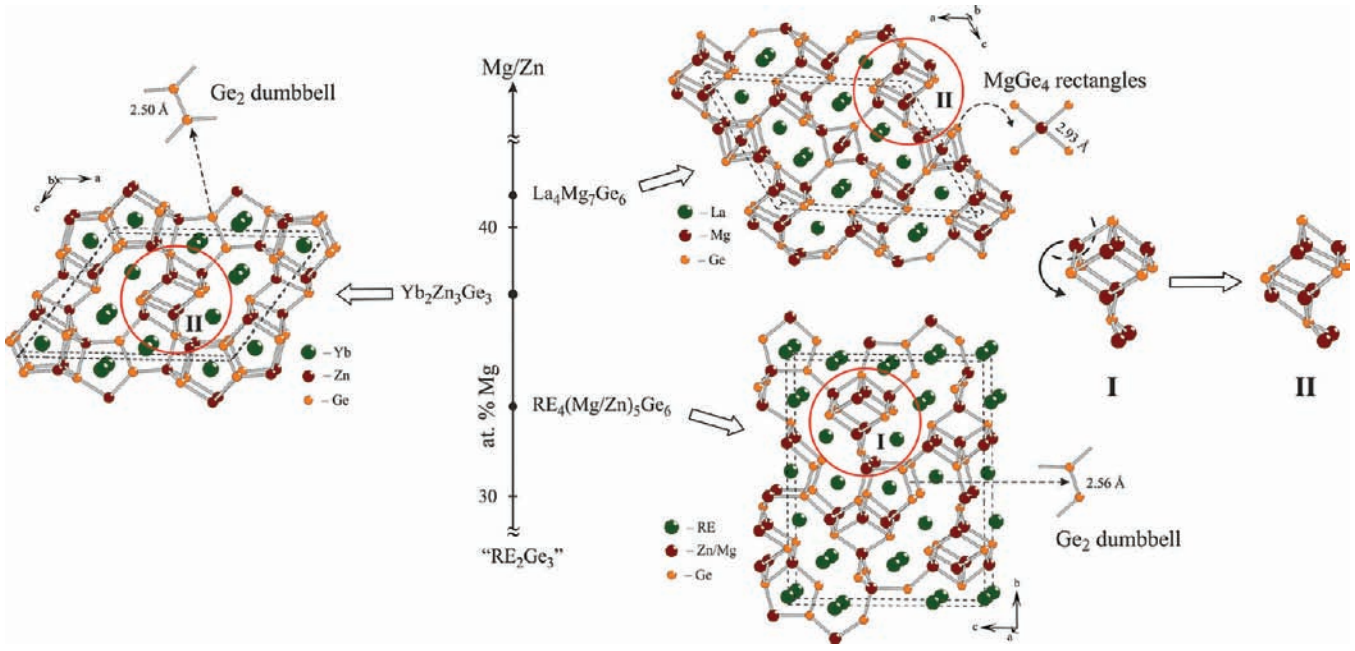

Figure 8. Polyanionic networks in RE–(Mg or Zn)–Ge phases with a 2:3 RE/Ge ratio.

dx.doi.org/10.1021/ic2014732 | *Inorg. Chem.* 2012, 51, 207–214

AUTHOR INFORMATION

Corresponding Author

*E-mail: pavlo.solokha@unige.it. Phone: +39-0103536159. Fax: +39-0103536163.

ACKNOWLEDGMENTS

The authors thank Dr. Giuseppe Fadda (Dipartimento di Fisica, Università di Cagliari) for valuable discussions on electronic structure calculations and interpretation of the results. Prof. Helmut Ehrenberg (Institute for Complex Materials, IFW Dresden) is acknowledged for providing access to single-crystal X-ray diffraction equipment.

REFERENCES

(1) Kauzlarich, S. M., Ed. *Chemistry, Structure and Bonding of Zintl Phases and Ions*; VCH Publishers: New York, 1996.
(2) Villars, P.; Cenzual, K. *Pearson's Crystal Data*; ASM International: Materials Park, OH, 2009/2010.
(3) Steinwand, S. J.; Hurng, W.-M.; Corbett, J. D. *J. Solid State Chem.* **1991**, *94*, 36.
(4) Eisenmann, B.; Schäfer, H. Z.; Weiss, A. *Z. Anorg. Allg. Chem.* **1972**, *391*, 241.
(5) Kraft, R.; Pöttgen, R. *Monatsh. Chem.* **2004**, *135*, 1327.
(6) Choe, W.; Miller, G. J.; Levin, E. M. *J. Alloys Compd.* **2001**, *329*, 121.
(7) De Negri, S.; Solokha, P.; Pavlyuk, V.; Saccone, A. *Intermetallics* **2011**, *19*, 671.
(8) Solokha, P.; De Negri, S.; Pavlyuk, V.; Eck, B.; Dronskowski, R.; Saccone, A. *J. Solid State Chem.* **2010**, *183*, 2995.
(9) Li, B.; Corbett, J. D. *Inorg. Chem.* **2006**, *45*, 3861.
(10) Li, B.; Corbett, J. D. *Inorg. Chem.* **2007**, *46*, 2237.
(11) Sheldrick, G. M. *SADABS: Siemens Area Detector Absorption Correction Software*; University of Goettingen: Goettingen, Germany, 1996.
(12) Sheldrick, G. M. *Acta Crystallogr.* **2008**, *A64*, 112.
(13) Spek, A. L. *PLATON, A Multipurpose Crystallographic Tool*; Utrecht University: Utrecht, The Netherlands, 2002.
(14) Andersen, O. K. *Phys. Rev. B* **1975**, *12*, 3060.
(15) Skriver, H. *The LMTO Method*; Springer-Verlag: Berlin, 1984.
(16) Andersen, O. K. In *The Electronic Structure of Complex Systems*; Phariseau, P., Temmerman, M., Eds.; Plenum: New York, 1984.
(17) Krier, G.; Jepsen, O.; Burkhardt, A.; Andersen, O. K. *The TB-LMTO-ASA program*, version 4.7; Max-Planck-Institut für Festkörperforschung: Stuttgart, Germany, 2000.
(18) von Barth, U.; Hedin, L. *J. Phys. C* **1972**, *5*, 1629.
(19) Dronskowski, R.; Blöchl, P. E. *J. Phys. Chem.* **1993**, *97*, 8617.
(20) Becke, A. D.; Edgecombe, K. E. *Nature* **1994**, *371*, 683.
(21) Eck, B. *wxDragon 1.7.1*; RWTH Aachen University: Aachen, Germany, 2010. Available at http://www.ssc.rwth-aachen.de.
(22) Gelato, L.; Parthé, E. *J. Appl. Crystallogr.* **1987**, *20*, 139.
(23) Kranenberg, C.; Johrendt, D.; Mewis, A. *Z. Anorg. Allg. Chem.* **2001**, *627*, 539.
(24) Sairanen, O. P.; Aksela, S.; Kivimaki, A. *J. Phys.: Condens. Matter* **1991**, *3*, 8707.
(25) U_{eq} is defined as one-third of the trace of the orthogonalized U_{ij} tensor.
(26) Xia, S.-Q.; Bobev, S. *J. Am. Chem. Soc.* **2007**, *129*, 10011.
(27) Li, B.; Corbett, J. D. *Inorg. Chem.* **2004**, *46*, 2237.
(28) You, T.-S.; Tobash, P. H.; Bobev, S. *Inorg. Chem.* **2010**, *49*, 1773.
(29) You, T.-S.; Bobev, S. *J. Solid State Chem.* **2010**, *183*, 1258.
(30) You, T.-S.; Bobev, S. *J. Solid State Chem.* **2010**, *183*, 2895.